




Article

Investigation of CeO₂, MoO₃, and Ce₂(MoO₄)₃, Synthesized by the Pechini Method, as Catalysts for Fructose Conversion

Dhara Beatriz de Amorim Pryston, Thatiane Veríssimo dos Santos Martins , Jailton Alves de Vasconcelos Júnior, Débora Olimpio da Silva Avelino, Mario Roberto Meneghetti  and Simoni Margareti Plentz Meneghetti * 

Group of Catalysis and Chemical Reactivity, Institute of Chemistry and Biotechnology, Federal University of Alagoas, Av. Lourival Melo Mota, Tabuleiro do Martins, Maceió 57072-970, AL, Brazil
* Correspondence: simoni.plentz@gmail.com; Tel.: +55-82-3214-1373

Abstract: Cerium oxide (Ce100), molybdenum oxide (Mo100), and a material containing Ce and Mo (CeMo) were synthesized by the Pechini method, using glycerol as a polyol. These materials were applied for fructose conversion in an aqueous medium. The characterization results show the formation of cerium molybdate (Ce₂(MoO₄)₃) for CeMo. Ce100 presented good thermal stability, and Mo100 sublimation of MoO₃ and polymolybdates was verified. CeMo exhibited a mass loss of 19%, associated with the sublimation of MoO₃ and polymolybdate species. Additionally, the existence of Bronsted and Lewis acid sites was confirmed, and the addition of Mo to Ce was an efficient strategy to increase the acidity. Regarding the catalytic activity (150 °C and 0.5 to 6 h), Ce100 exhibited low conversions and high selectivity to 5-hydroxymethylfurfural (5-HMF). For Mo100, high conversions, with a significant formation of insoluble materials, were detected. For CeMo, beyond the high activity, a lower formation of insoluble materials was noted. In this case, selectivity toward products from the retro-aldolic route and 5-HMF were obtained. These results indicate that the main factor influencing fructose conversion is an adequate combination of the acid sites. Recycling experiments were carried out, and stability was observed for four cycles, confirming the robustness of this system.

Keywords: cerium oxide; molybdenum oxide; cerium molybdate; biomass; biorefinery



Citation: Pryston, D.B.d.A.; Martins, T.V.d.S.; Vasconcelos Júnior, J.A.d.; Avelino, D.O.d.S.; Meneghetti, M.R.; Meneghetti, S.M.P. Investigation of CeO₂, MoO₃, and Ce₂(MoO₄)₃, Synthesized by the Pechini Method, as Catalysts for Fructose Conversion. *Catalysts* **2023**, *13*, 4. <https://doi.org/10.3390/catal13010004>

Academic Editors: Linda Zh Nikoshvili, Victorio Cadierno, Liubov Kiwi-Minsker and Valentin Yu Doluda

Received: 9 November 2022

Revised: 14 December 2022

Accepted: 16 December 2022

Published: 20 December 2022



Copyright: © 2022 by the authors. Licensee MDPI, Basel, Switzerland. This article is an open access article distributed under the terms and conditions of the Creative Commons Attribution (CC BY) license (<https://creativecommons.org/licenses/by/4.0/>).

1. Introduction

The environmental and social problems caused by the dependence of the global energy matrix and the chemical synthesis on fossil fuels (oil, coal, and natural gas) motivated the search for sustainable energy sources, with an emphasis on biomass [1–3]. Regarding biomass-derived inputs, special attention is directed to carbohydrates, such as fructose, since the conversion of these molecules provides the formation of a spectrum of valuable chemicals [4], including 5-hydroxymethylfurfural [5] and lactic acid [6].

Catalysis is strategic in the transformation of biomass, mainly because it influences the selectivity to the desired product and thus minimizes the generation of byproducts. The development of heterogeneous catalysts is a key resource for sustainable advancement due to its associated advantages, such as easy recovery and reuse. From this perspective, metal oxides have been widely explored due to their acid/base and redox characteristics, as well as the presence of structural defects. These parameters are very important for academic and industrial applications; moreover, these materials are affordable [3,7–12].

The unique properties of cerium- and molybdenum-based materials justify their various catalytic applications. Cerium oxide exhibits outstanding physical and chemical stability, ease of reduction or oxidation (Ce³⁺ ↔ Ce⁴⁺), and high electron mobility in the crystal lattice [8,13,14]. Molybdenum oxide is known to be an efficient modulator of acidity [15]. The presence of Lewis and Bronsted acid sites directly influences the conversion of carbohydrates [11].

The junction of metal oxides can lead to attractive changes in physical, chemical, and catalytic properties [8]. This fact allows for the development in this study of a promising

catalytic system using cerium and molybdenum for carbohydrate conversion. Although the application of cerium molybdate—exhibiting contributions in photocatalysis [16], gas detection [12], antiviral activity [17], and catalysis [18]—in diverse areas is extensive, to date, no information has been found on its evaluation in the conversion of hexoses. Several synthesis routes, including the precipitation method [19], wet impregnation [15,20], and hydrothermal methods [21], can be used for the preparation of metal oxides. However, the Pechini method has been noted as one of the most promising methodologies for obtaining heterogeneous catalysts because it requires low cost and the use of mild temperatures, as well as being considered a simple process [22]. The basic procedure of the synthesis consists of the formation of a polymeric resin in which the cations are homogeneously dispersed through a reaction between a polycarboxylic acid (such as citric acid), metal ions, and a polyol [23–26]. Ethylene glycol is commonly used as a polymerizing agent in the Pechini method [22,27]. However, this compound presents toxicity and is generated largely by fossil fuel sources [28,29]. On the other hand, glycerol is a nontoxic product, and it can be obtained renewably; a possible replacement of polyol may assign a more sustainable footprint to this route [24,30,31].

Therefore, this study proposed to synthesize cerium oxide (CeO_2), molybdenum oxide (MoO_3), and a mixed oxide based on Mo and Ce through the modified Pechini method, using glycerol as a polymerizing agent. For the first time, such materials, after characterization, were evaluated in the conversion of fructose to chemical inputs of industrial interest.

2. Results and Discussion

The catalysts Ce100, Mo100, and Ce Mo were used in the conversion of fructose in an aqueous medium, and the results are shown in Figure 1. Initially, the experiments showed that Ce100 leads to low conversions, comparable to those obtained in the reaction carried out without the addition of a catalyst. However, in the presence of Mo100 and CeMo, higher conversions were observed, especially for Mo100. For example, at 3 h of reaction, the observed values of conversion were 97.4 and 91.8% for Mo100 and CeMo, respectively. After 4 h of reaction, the two systems led to very close conversions, and the system tended to reach equilibrium.

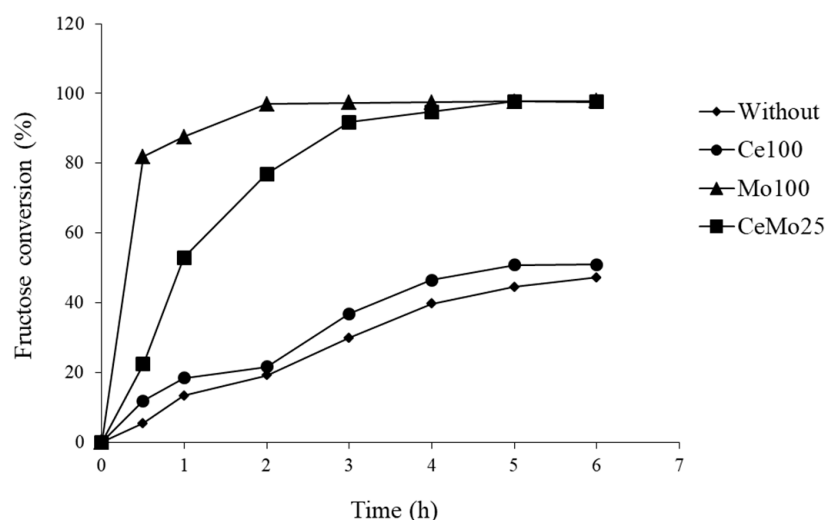


Figure 1. Fructose conversion at 150 °C without a catalyst or with 1.5×10^{-3} g of Ce100, Mo100, or CeMo.

Such conversions may be related to the properties of these catalytic systems, and Table 1 presents some results regarding the characterization and evaluation of the acid sites.

Table 1. Textural and structural properties of the solids investigated in this study.

Sample	S_{BET}^a ($\text{m}^2\cdot\text{g}^{-1}$)	Crystallite Size (nm) ^b	Amount Bronsted ^c ($\text{mmol}\cdot\text{g}^{-1}$)	Amount Lewis ^c ($\text{mmol}\cdot\text{g}^{-1}$)	$A_{\text{B}}/A_{\text{L}}^d$
Ce100	70.6	10.1	157.5	120.0	1.3
Mo100	>5.0	133.6	700.0	531.8	1.3
CeMo	>5.0	40.5	490.7	291.1	1.7

^a S_{BET} , specific surface area, calculated by the BET equation. ^b Crystallite size (nm) calculated by the Debye–Scherrer equation. ^c Number of Lewis and Bronsted acid sites ($\text{mmol}\cdot\text{g}^{-1}$), obtained from FTIR spectra using pyridine as the probe molecule. ^d Ratio of the number of Lewis and Bronsted acid sites.

The low conversion obtained in the presence of Ce100 can be explained by the fact that, even with a surface area much larger than that observed for the other systems investigated here, there is a smaller number of Bronsted and Lewis acid sites in the structure of this material. In the case of the other two systems, higher numbers of acid sites were observed, which justifies the higher conversions, despite the low surface areas. Furthermore, it is important to note that in the CeMo catalyst, the $A_{\text{B}}/A_{\text{L}}$ ratio is superior to the other pure oxides, indicating a higher incidence of Bronsted acid sites in this material.

Previous study data indicate that the number of Lewis and Bronsted acid sites available in the catalyst is related to the success of this type of conversion, and the synergism resulting from the combination between these sites is responsible for obtaining promising results in terms of converting carbohydrates into molecules of interest [8,32,33]. For example, in the synthesis of the mixed oxides of molybdenum and tin, increasing the content of molybdenum in relation to tin increases the acidity, leading to high fructose conversions, with selectivity to the products obtained by retro-aldol and dehydration reactions [11].

Regarding the soluble products identified (see Figure 2) in the presence of Mo100, there is no defined selectivity, although in the first few hours of reaction, this system is the most active of all. In contrast, in the presence of Ce100, a great selectivity to HMF and to products and intermediates of the retro-aldol pathway is observed (glyceraldehyde, dihydroxyacetone, pyruvaldehyde, and lactic acid). However, the latter showed maximum conversions of 50% between 5 and 6 h of reaction. For CeMo, a change in the selectivity profile is observed, with a majority targeting the retro-aldol pathways (pyruvaldehyde, glyceraldehyde, lactic acid, and acetic acid), isomerization (glucose), and dehydration (5-HMF).

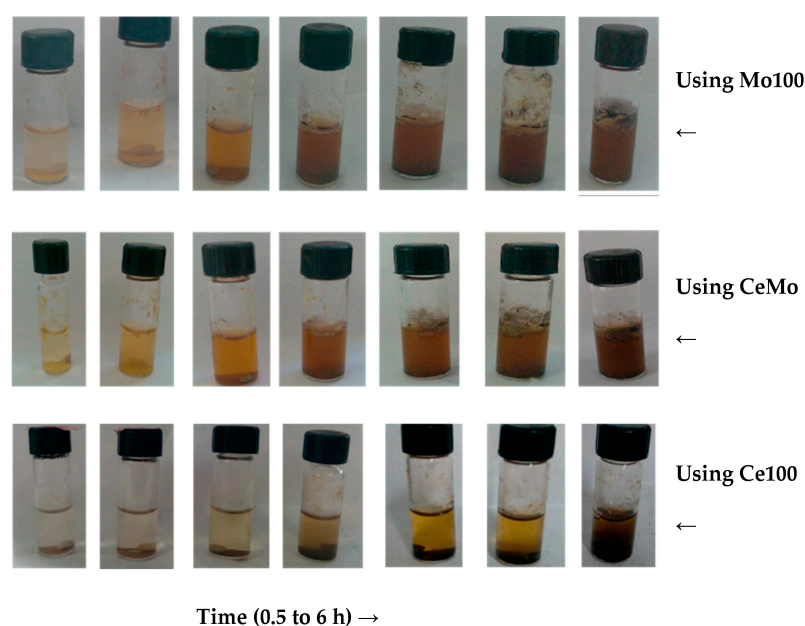


Figure 2. Visual aspects of the samples during the reaction, using catalysts (1.5×10^{-3} g) at $150\text{ }^\circ\text{C}$ (0.5 to 6 h).

The formation of 5-HMF follows the route of dehydration of the fructose molecule, which occurs through the consecutive loss of three water molecules. However, due to the high instability of 5-HMF in aqueous media, organic acids are formed, as well as humins [34,35]. The Ce100 catalyst showed high selectivity (70.2% at 6 h) for 5-HMF. On the other hand, the Mo100 and CeMo systems exhibited lower selectivity for this product under the same conditions, 14.5% and 27.5%, respectively. This fact can be explained by the formation of organic acids (levulinic and formic) through the hydration of 5-HMF [34]. It should be noted that for Ce100, no levulinic or formic acid was identified, and this fact can be associated with the nature of the acid sites associated with this catalyst [36]. The literature reports that the decomposition of 5-HMF into organic acids and other side reactions are favored when there are higher numbers of acidic sites in the catalyst [11,37,38]. As shown in Table 2, CeMo and Mo100 contain more of these sites when compared to Ce100. However, for Ce100 and CeMo, the increase in fructose conversion implies an increase in 5-HMF selectivity, a characteristic that is not observed for Mo100.

Table 2. Ranges of thermal decomposition for Ce100, Mo100, and CeMo.

Range T (°C)	Ce100	Mo100	CeMo
100–150	2.3	nd	nd
700–850	2.7	78.2	nd
850–1000	nd	17.5	nd
>1000	2.4	nd	19.0

nd = not detected.

The reduced selectivity to 5-HMF, mainly with the use of Mo100 (14.5%) and CeMo (27.5%) compared to Ce100 (70.2%), may also be associated with the formation of humins, promoted by the condensation between 5-HMF and other reaction intermediates and which is closely related to the conditions used and the acidity of the catalyst [36,39]. The presence of this byproduct can be quantitatively identified through the color change of the reaction medium, that is, the evolution to a dark brown color [36]. As shown in Figure 3, there was a greater formation of humins for Mo100 due to the high acidity of the material (Table 2). For CeMo, a lower and adequate acidity inhibited the high generation of these byproducts. The same justification can be used for Ce100; however, the lower number of acid sites also directly influenced the catalyst activity (see Figure 1). Such observations suggest that a possible structural change, in relation to the pure oxides, obtained in the case of CeMo leads to a better conversion of fructose, maintaining the advantage in terms of the formation of a smaller amount of insoluble products when compared to Mo100.

Lactic acid is a product widely used in the food, chemical, pharmaceutical, and cosmetics industries [40]. When using CeMo and Ce100, a high selectivity was observed for pyruvaldehyde (lactic acid precursor) in the initial reaction times up to 2 h. With longer reaction times, the selectivity to pyruvaldehyde decreases as lactic acid is formed. Interestingly, for Ce100, the presence of glyceraldehyde is notable at lower levels than those of the other precursors, suggesting that the conversion reaction of the product to pyruvaldehyde is very rapid [41]. Previous studies report that the Bronsted and Lewis acid sites are fundamental in promoting the formation of lactic acid, with the first acting on the dehydration of triose to pyruvaldehyde and the second promoting the conversion of pyruvaldehyde to lactic acid through the 1,2 displacement of hydride [42,43].

As shown in Figure 2, Mo100 showed greater selectivity for lactic acid and its intermediates due to the greater number of Lewis acid sites in its structure, which enabled the conversion of pyruvaldehyde. Similarly, this explanation is also useful in relation to the greater selectivity of CeMo to lactic acid when compared to Ce100. This suggests that the lower Lewis acidity and considerable number of Bronsted acid sites present in CeMo and Ce100 led to higher selectivities to pyruvaldehyde in the initial reaction times.

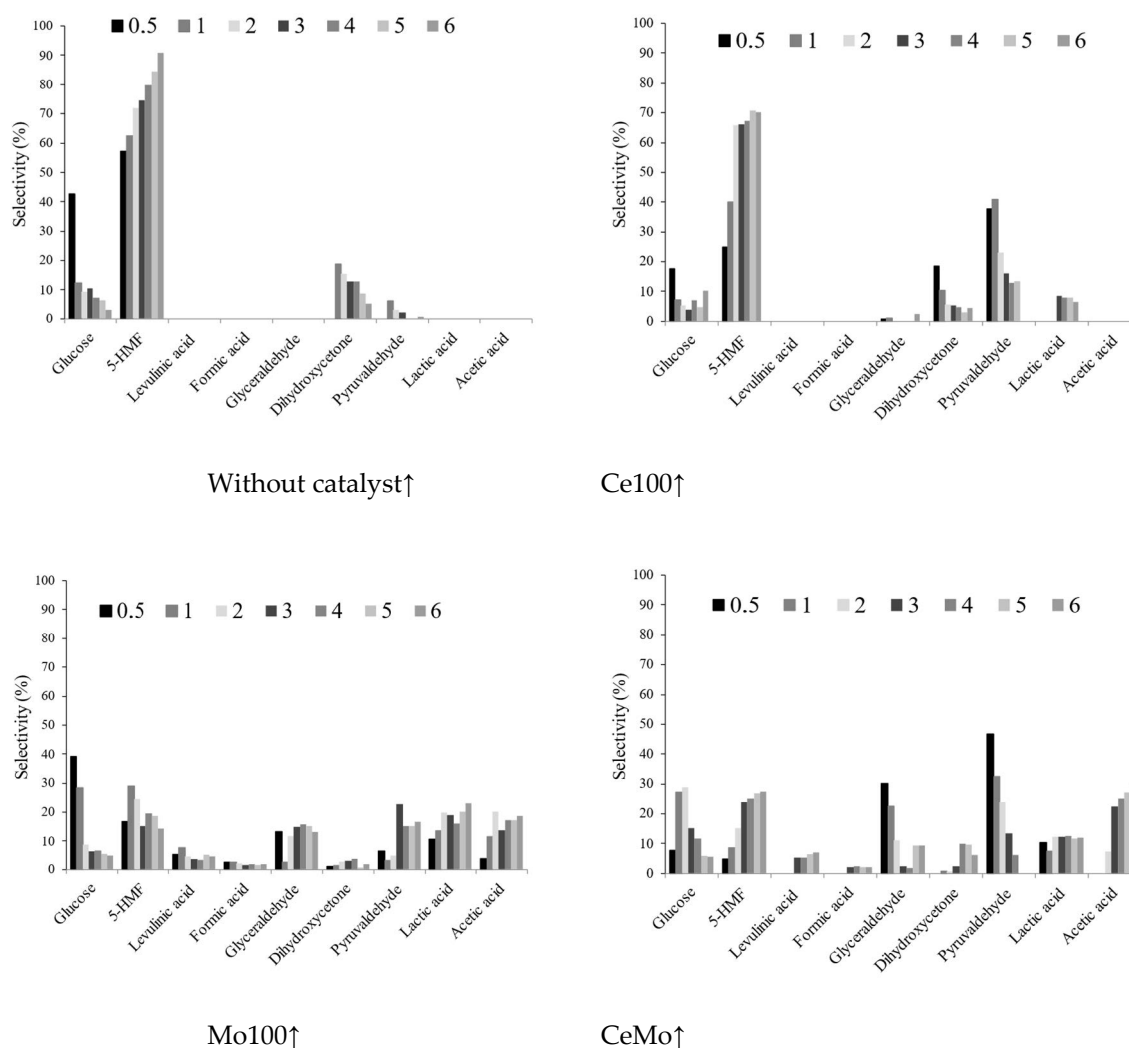


Figure 3. Selectivity for soluble products identified in the fructose conversion at 150 °C, without a catalyst and with 1.5×10^{-3} g of Ce100, Mo100, and CeMo.

Acetic acid is one of the products in high demand in the chemical industry, and it is used as a precursor for various chemical compounds [44,45]. Its most common formation route from the biomass is the retro-aldolic pathway [11,24]. When Ce100 was used as a catalyst, the presence of this compound was not observed, since the decomposition route for the formation of acetic acid is directed by the Lewis acid sites, which were also not identified when Ce100 was used [46]. Furthermore, a greater selectivity of CeMo (29.9%) to acetic acid was observed in relation to Mo100 (18.8%) at 6 h. This result suggests a greater suitability of sites in CeMo, while the greater acidity of Mo100 led to other parallel reactions.

The characterization of these materials, obtained through the Pechini method by using glycerol instead of ethylene glycol, by XRD revealed that cerium molybdate ($\text{Ce}_2(\text{MoO}_4)_3$) was formed in the case of the CeMo material (Figure 4), and no signals referring to the individual oxides were identified. The formation of ($\text{Ce}_2(\text{MoO}_4)_3$) was confirmed by the crystalline planes assigned to the reflection lines (002) (100) (101) (112) (004) (200) (211) (204) (220) (116) (312) (224) (card # 30-0303) [17]. As shown in Figure 4, Ce100 exhibits a fluorite-like (CaF_2) face-centered cubic structure, according to the JCPDS crystallographic sheet No. 34-0394 [8,13,21]. Mo100 showed all peaks perfectly indexed, suggesting the formation of the orthorhombic phase (JCPDS No. 05-0508).

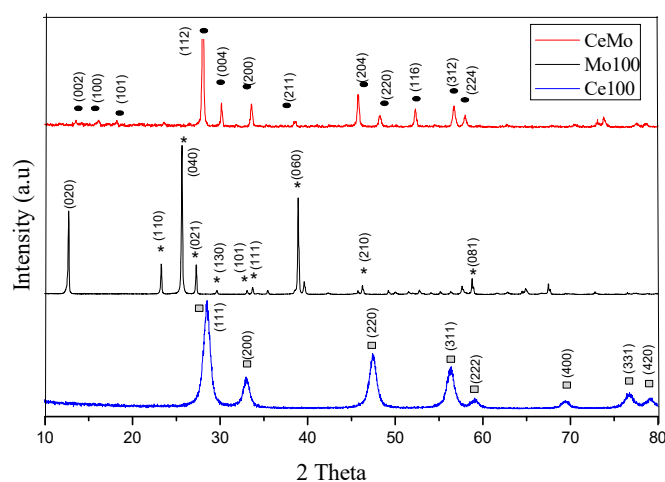


Figure 4. XRD patterns of Ce100 (● = fluorite-like face-centered cubic structure (JCPDS 34-0394)), Mo100 (* = orthorhombic phase (JCPDS No. 05-0508)), and CeMo (□ = $\text{Ce}_2(\text{MoO}_4)_3$ (JCPDS 30-0303)).

Based on the information extracted from the diffractograms, the crystallite size (see Table 1) was calculated using the Debye–Scherrer equation, and for this, the most intense diffraction peaks of CeMo, Ce100, and Mo100 were used, e.g., (112), (040), and (111), respectively. Therefore, the diffractograms show that the addition of molybdenum leads to an increase in crystallite size, suggesting crystal growth by particle aggregation because of mixed oxide formation [15]. This fact also corroborates the result obtained by the BET method, from which a pronounced reduction in the specific surface area was observed (see Table 1).

The structural changes that occurred by the formation of $\text{Ce}_2(\text{MoO}_4)_3$, in relation to the individual oxides, were confirmed by the evaluation of thermal behavior. In the thermogram obtained for CeMo (Table 2 and Figure S1, Supplementary Materials), only one thermal decomposition event was observed above 1000 °C (with a mass loss of 19%), which clearly continues to occur, but which is not quantified due to the limitation of the equipment, which operates at a maximum temperature of 1500 °C. This suggests that the interaction between the molybdenum and cerium ions for the formation of cerium molybdate leads to an increase in thermal stability, and the mass loss above 850 °C is associated with the decomposition of the material into cerium and molybdenum oxide and the subsequent sublimation of MoO_3 [47–49]. Reports indicate that in this type of material, when subjected to temperatures above 700 °C, defects are formed that favor greater mobility of the molybdenum and cerium ions, consequently leading to changes in the mutual interaction between them, leading to increased thermal stability [48].

Three thermal decomposition events were observed in Ce100 (Figure S1, Supplementary Materials). The first event (mass loss of 2.3%) is attributed to the desorption of water molecules (Khalil et al., 2005). The second event starts at 730 °C (mass loss of 2.7%) and can be related to the oxygen output from the oxide structure [50,51]. The total mass loss recorded after heating from 25 °C to 1500 °C was 7.4%, suggesting good thermal stability. In the case of Mo100 (see Figure S1, Supplementary Materials), two thermal decomposition events were observed. The first, which occurs in the range of 700–850 °C (mass loss of 78.2%), corresponds to the sublimation of MoO_3 . The second occurs between 850–1000 °C (mass loss of 17.5%) and can be associated with the output of polymolybdates [11].

Therefore, it can be inferred that the synthesis of the material from the molybdenum and cerium precursors, under the conditions used here, is an efficient strategy for the modulation of acid sites, resulting in a suitable catalytic system for the conversion of fructose into an aqueous medium. The formation of insoluble byproducts is minimized when compared to Mo100, leading to promising conversions, mainly after 3 h of reaction under the conditions investigated here. In addition, a superior thermal stability of CeMo was observed in relation to Mo100.

Catalyst recyclability is of great importance in biorefinery processes [11]. In this study, the catalyst was calcined to eliminate organic fractions and perform reuse tests (1 h, 1.5×10^{-3} g of catalyst, 150 °C). The results of the recycling experiments are shown in Figure 5, and only a small variation in conversion and selectivity values was observed for CeMo for each of the 4 cycles tested (approximately 72.0% of conversion, on average). The liquid samples collected after the first and the last (4th) cycle were subjected to X-ray dispersive energy spectrometry (EDX) analysis, and no significant amount of molybdenum or cerium was detected, suggesting that leaching did not occur.

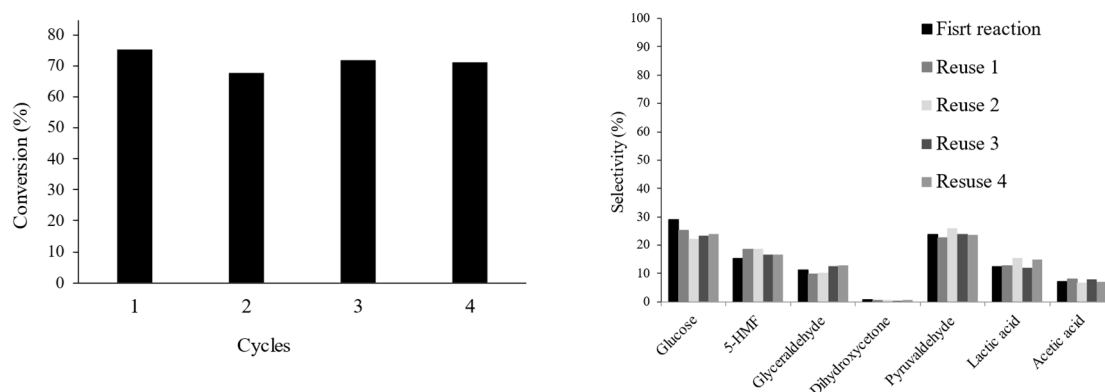


Figure 5. Results of reuse for the CeMo system (150 °C, 1 h).

3. Materials and Methods

3.1. Materials

Ammonium heptamolybdate tetrahydrate (99.9%, Sigma-Aldrich, St. Louis, MI, USA), cerium(III) nitrate hexahydrate (99.9%, Sigma-Aldrich), citric acid (>99.0%, Sigma-Aldrich), ammonium hydroxide (Sigma-Aldrich), nitric acid (>65.0%, Sigma-Aldrich), glycerol (>99.0%, Sigma-Aldrich), and fructose (>99.0%, Sigma-Aldrich) were obtained commercially and used as received.

3.2. Synthesis and Characterization

Initially, citric acid and the metal precursor were weighed in a molar ratio of 3:1. Then, both were dissolved separately in deionized water at 30 °C under constant stirring and mixed for 30 min. The next step was the addition of glycerol to the prepared solution in a molar ratio of 60:40, based on the amount of citric acid, maintaining vigorous stirring at 70 °C for 3 h to ensure the homogeneity of the system. Subsequently, the temperature was increased to 130 °C to promote the polyesterification reaction and the subsequent formation of the polymeric resin. The metal precursors used were cerium(III) nitrate hexahydrate and ammonium heptamolybdate [24,31]. The mixed catalyst was prepared in a mass ratio of 75% cerium to 25% molybdenum, and cerium(III) nitrate hexahydrate and ammonium heptamolybdate were weighed and dissolved separately in deionized water at 30 °C under constant stirring. Soon after, both were mixed and added to a beaker containing a solution of citric acid, maintained under vigorous stirring for 30 min. All the following procedures were identical to those described above for the pure oxides. The materials were subjected to heat treatment at 280 °C for 2 h, using a heating rate of 10 °C/min to break the polymer chains and form a semicarbonized black powder. Subsequently, they were macerated in a mortar and sieved (100 mesh) to be placed again in the muffle furnace at 550 °C for 4 h. Finally, all materials were stored under an argon atmosphere. Table 3 presents the description of the catalysts and the codes used.

Table 3. Code of the catalysts and the respective descriptions.

Code	Description
Ce100	Cerium oxide(IV) (CeO ₂)
Mo100	Molybdenum oxide(VI) (MoO ₃)
CeMo	Cerium molybdate (Ce ₂ (MoO ₄) ₃)

For material characterization, X-ray diffraction (XRD) measurements were performed using a Shimadzu diffractometer, model XRD-6000, and a Cu K α radiation source (1.5418 Å) with a nickel filter to obtain wide-angle diffraction patterns in the $2\theta = 3\text{--}40^\circ$ range. Crystallite size (nm) was calculated using the Debye–Scherrer equation.

Nitrogen adsorption measurements were performed at 77.15 K using a gas adsorption analyzer (Micromeritics, model ASAP-2020). The textural properties were estimated from the N₂ adsorption isotherms using the Brunauer–Emmett–Teller (BET) equation and the Barrett–Joyner–Halenda (BJH) method. Before the analysis, all the samples were pretreated under vacuum at 423.15 K for 24 h. Thermogravimetric (TG/DTG) analyses were performed using a Shimadzu analyzer, model DTG-60H, with an N₂ flow rate of 40 mL·min^{−1} in the temperature range of 30–800 °C at a heating rate of 10 °C·min^{−1}. Fourier transform infrared (FTIR) spectra were obtained with a Shimadzu IR Prestige 21 infrared spectrophotometer using potassium bromide tablets (KBr). A total of 80 scans were performed in the transmittance mode in the spectral range of 4000–400 cm^{−1} at a resolution of 4.0 cm^{−1}.

3.3. Conversion of Fructose

All experiments were performed in 4 mL vials under magnetic stirring and heating (150 °C), at several reaction times. The fructose solution was 0.016 g of fructose in 2 mL of deionized water, and for some experiments, catalysts (1.5×10^{-3} g) were used. Conversion, yield, and selectivity were calculated from the results of quantification by HPLC. The reuse tests of CeMo (G) were carried out at 150 °C for 2 h under the same reaction conditions. Subsequently, the catalyst was removed from the reaction medium by centrifugation and calcined at 550 °C for 4 h for subsequent reuse. The liquid samples collected after the cycles were subjected to X-ray dispersive energy spectrometry (EDX) analysis to determine whether leaching had occurred.

4. Conclusions

In the absence of a catalyst or using Ce100, low fructose conversions were observed, with the formation mainly of 5-HMF. In contrast, in the presence of Mo100 and CeMo, higher conversions are achieved, and the formation of different products was observed. However, using Mo100, which exhibits a higher number of Lewis and Bronsted acid sites than does CeMo, higher conversions were observed before the achievement of thermodynamic equilibrium, but this is accompanied by the formation of a greater amount of soluble and insoluble material, directly reflected in the color evolution of the reactions over time. In relation to the soluble products formed from fructose using CeMo, the direction to the retro-aldolic pathway was observed, evidencing the modulation of these systems. It is important to highlight that the low conversion obtained in the presence of Ce100 can be explained by the smaller number of Bronsted and Lewis acid sites in the structure of this material, even with a surface area much higher than that observed for the other systems. In the case of Mo100 and CeMo, higher levels of acid sites were observed, which justifies the higher conversions, despite the low surface areas. Reuse and leaching tests indicated that the CeMo system proved to be stable and robust under the conditions tested.

Supplementary Materials: The following supporting information can be downloaded at: <https://www.mdpi.com/article/10.3390/catal13010004/s1>, Figure S1: Thermogravimetric analysis (TG/DTG): (A) Ce100, (B) Mo100, and (C) CeMo.

Author Contributions: Conceptualization, D.B.d.A.P., M.R.M. and S.M.P.M.; methodology, D.B.d.A.P., T.V.d.S.M., J.A.d.V.J. and D.O.d.S.A.; investigation, D.B.d.A.P., T.V.d.S.M., J.A.d.V.J., M.R.M. and S.M.P.M.; resources, M.R.M. and S.M.P.M.; writing—original draft preparation, D.B.d.A.P., T.V.d.S.M. and S.M.P.M.; writing—review and editing, D.B.d.A.P., T.V.d.S.M., M.R.M. and S.M.P.M.; visualization, D.B.d.A.P., T.V.d.S.M., J.A.d.V.J., M.R.M. and S.M.P.M.; supervision, M.R.M. and S.M.P.M.; project administration, M.R.M. and S.M.P.M.; funding acquisition, M.R.M. and S.M.P.M. All authors have read and agreed to the published version of the manuscript.

Funding: This research was supported by the National Council for Scientific and Technological Development (CNPq), the Brazilian Federal Agency for the Improvement of Higher Education (CAPES), the Brazilian Innovation Agency (FINEP), and the Alagoas Research Foundation (FAPEAL). G.C.A. and I.M.A.S. express their appreciation for fellowships granted by CAPES and CNPq. M.R.M. and S.M.P.M. thank CNPq for research fellowships.

Data Availability Statement: Not applicable.

Acknowledgments: The authors also thank the LSCAT/CTEC/UFAL, TecNano/ICF/UFAL, and GON/IF/UFAL teams for their contributions.

Conflicts of Interest: The authors declare no conflict of interest.

References

1. Huang, H.; Gao, Y.; Chen, H.; Wu, Y.; Wang, J.; Yu, C.; Li, J.; Zou, C. Biomass Briquette Fuel, Boiler Types and Pollutant Emissions of Industrial Biomass Boiler: A Review. *Particuology* **2022**, *77*, 79–90. [[CrossRef](#)]
2. Gani, A. Fossil Fuel Energy and Environmental Performance in an Extended STIRPAT Model. *J. Clean. Prod.* **2021**, *297*, 126526. [[CrossRef](#)]
3. Deng, W.; Feng, Y.; Fu, J.; Guo, H.; Guo, Y.; Han, B.; Jiang, Z.; Kong, L.; Li, C.; Liu, H.; et al. Catalytic Conversion of Lignocellulosic Biomass into Chemicals and Fuels. *Green Energy Environ.* **2022**; *in press*. [[CrossRef](#)]
4. Bayu, A.; Abudula, A.; Guan, G. Reaction Pathways and Selectivity in Chemo-Catalytic Conversion of Biomass-Derived Carbohydrates to High-Value Chemicals: A Review. *Fuel Process. Technol.* **2019**, *196*, 106162. [[CrossRef](#)]
5. Mehta, J.; Metre, A.V.; Bhakhar, M.S.; Panwar, D.S.; Dharaskar, S. Biomass-Derived 5-Hydroxymethylfurfural (HMF) and 2,5-Dimethylfuran (DMF) Synthesis as Promising Alternative Fuel: A Prospective Review. *Mater. Today Proc.* **2022**, *62*, 6978–6984. [[CrossRef](#)]
6. Li, Y.; Ma, J.; Jin, D.; Jiao, G.; Yang, X.; Liu, K.; Zhou, J.; Sun, R. Copper Oxide Functionalized Chitosan Hybrid Hydrogels for Highly Efficient Photocatalytic-Reforming of Biomass-Based Monosaccharides to Lactic Acid. *Appl. Catal.* **2021**, *291*, 120123. [[CrossRef](#)]
7. Védrine, J.C. Metal Oxides in Heterogeneous Oxidation Catalysis: State of the Art and Challenges for a More Sustainable World. *ChemSusChem* **2019**, *12*, 577–588. [[CrossRef](#)]
8. Stošić, D.; Bennici, S.; Rakić, V.; Auroux, A. CeO₂-Nb₂O₅ Mixed Oxide Catalysts: Preparation, Characterization and Catalytic Activity in Fructose Dehydration Reaction. *Catal. Today* **2012**, *192*, 160–168. [[CrossRef](#)]
9. Gawande, M.B.; Pandey, R.K.; Jayaram, R.V. Role of Mixed Metal Oxides in Catalysis Science—Versatile Applications in Organic Synthesis. *Catal. Sci. Technol.* **2012**, *2*, 1113. [[CrossRef](#)]
10. Xu, S.; Pan, D.; Li, W.; Shen, P.; Wu, Y.; Song, X.; Zhu, Y.; Xu, N.; Gao, L.; Xiao, G. Direct Conversion of Biomass-Derived Carbohydrates to 5-Hydroxymethylfurfural Using an Efficient and Inexpensive Manganese Phosphate Catalyst. *Fuel Process. Technol.* **2018**, *181*, 199–206. [[CrossRef](#)]
11. Dos Santos, T.V.; Da Silva Avelino, D.O.; Meneghetti, M.R.; Meneghetti, S.M.P. Mixed Oxides Based on SnO₂ Impregnated with MoO₃: A Robust System to Apply in Fructose Conversion. *Catal. Commun.* **2018**, *114*, 120–123. [[CrossRef](#)]
12. Oliveira, F.K.F.; Santiago, A.A.G.; Catto, A.C.; da Silva, L.F.; Tranquilin, R.L.; Longo, E.; Motta, F.V.; Bomio, M.R.D. Cerium Molybdate Nanocrystals: Microstructural, Optical and Gas-Sensing Properties. *J. Alloy. Compd.* **2021**, *857*, 157562. [[CrossRef](#)]
13. Chen, B.; Li, P.; Wang, B.; Wang, Y. Flame-Annealed Porous TiO₂/CeO₂ Nanosheets for Enhanced CO Gas Sensors. *Appl. Surf. Sci.* **2022**, *593*, 153418. [[CrossRef](#)]
14. Benali, F.; Boukoussa, B.; Ismail, I.; Hachemaoui, M.; Iqbal, J.; Taha, I.; Cherifi, Z.; Mokhtar, A. One Pot Preparation of CeO₂@Alginate Composite Beads for the Catalytic Reduction of MB Dye: Effect of Cerium Percentage. *Surf. Interfaces* **2021**, *26*, 101306. [[CrossRef](#)]
15. Assis, G.C.; Silva, I.M.A.; Dos Santos, T.V.; Meneghetti, M.R.; Meneghetti, S.M.P. Photocatalytic Properties of SnO₂/MoO₃ Mixed Oxides and Their Relation to the Electronic Properties and Surface Acidity. *J. Photochem. Photobiol.* **2021**, *407*, 113035. [[CrossRef](#)]
16. Muthuvel, I.; Sathyapriya, S.; Suguna, S.; Gowthami, K.; Thirunarayanan, G.; Rajalakshmi, S.; Sundaramurthy, N.; Dinesh Karthik, A.; Rajachandrasekar, T. Solar Light Driven Cerium Molybdate Nanocatalyst for Effective Photodecomposition of Fuchsin Basic Dye. *Mater. Today Proc.* **2021**, *43*, 2274–2279. [[CrossRef](#)]

17. Ito, T.; Sunada, K.; Nagai, T.; Ishiguro, H.; Nakano, R.; Suzuki, Y.; Nakano, A.; Yano, H.; Isobe, T.; Matsushita, S.; et al. Preparation of Cerium Molybdates and Their Antiviral Activity against Bacteriophage $\Phi 6$ and SARS-CoV-2. *Mater. Lett.* **2021**, *290*, 129510. [[CrossRef](#)]
18. Liu, X.-Y.; Li, X.-P.; Zhao, R.-X. $\text{Ce}_2(\text{MoO}_4)_3$ as an Efficient Catalyst for Aerobic Oxidative Desulfurization of Fuels. *Pet. Sci.* **2022**, *19*, 861–869. [[CrossRef](#)]
19. Putri, G.E.; Rilda, Y.; Syukri, S.; Labanni, A.; Arief, S. Highly Antimicrobial Activity of Cerium Oxide Nanoparticles Synthesized Using Moringa Oleifera Leaf Extract by a Rapid Green Precipitation Method. *J. Mater. Res. Technol.* **2021**, *15*, 2355–2364. [[CrossRef](#)]
20. Hadebe, N.P.; Kerru, N.; Tukulula, M.; Jonnalagadda, S.B. A Sustainable Molybdenum Oxide Loaded on Zirconia ($\text{MoO}_3/\text{ZrO}_2$) Catalysed Multicomponent Reaction to Synthesize Novel Dihydropyridines. *Sustain. Chem. Pharm.* **2022**, *25*, 100578. [[CrossRef](#)]
21. Afza, N.; Shivakumar, M.S.; Alam, M.W.; Kumar, A.N.; Bhatt, A.S.; Murthy, H.C.A.; Ravikumar, C.R.; Mylarappa, M.; Selvanandan, S. Facile Hydrothermal Synthesis of Cerium Oxide/RGO Nanocomposite for Photocatalytic and Supercapacitor Applications. *Appl. Surf. Sci.* **2022**, *11*, 100307. [[CrossRef](#)]
22. Garcia, A.B.S.; Bispo-Jr, A.G.; Lima, S.A.M.; Pires, A.M. Effects of the Pechini's Modified Synthetic Route on Structural and Photophysical Properties of Eu^{3+} or Tb^{3+} -Doped LaAlO_3 . *Mater. Res. Bull.* **2021**, *143*, 111462. [[CrossRef](#)]
23. Wang, Y.; Li, H.; Huang, D.; Wang, X.; Cai, L.; Chen, Y.; Wang, W.; Song, Y.; Han, G.; Zhen, B. A High-Performance Ethanol Gas Sensor Based on Ce-Doped SnO_2 Nanomaterials Prepared by the Pechini Method. *Mater. Sci. Semicond. Process.* **2022**, *137*, 106188. [[CrossRef](#)]
24. Dos Santos, T.V.; Pryston, D.B.A.; Assis, G.C.; Meneghetti, M.R.; Meneghetti, S.M.P. Tin, Niobium and Tin-Niobium Oxides Obtained by the Pechini Method Using Glycerol as a Polyol: Synthesis, Characterization and Use as a Catalyst in Fructose Conversion. *Catal. Today* **2021**, *379*, 62–69. [[CrossRef](#)]
25. Kang, J.; Gwon, Y.R.; Cho, S.K. Photoelectrochemical Water Oxidation on PbCrO_4 Thin Film Photoanode Fabricated via Pechini Method: Various Solution-Processes for PbCrO_4 Film Synthesis. *J. Electroanal. Chem.* **2020**, *878*, 114601. [[CrossRef](#)]
26. Mahdi, M.A.; Jasim, L.S.; Ranjeh, M.; Masjedi-Arani, M.; Salavati-Niasari, M. Improved Pechini Sol-Gel Fabrication of $\text{Li}_2\text{B}_4\text{O}_7/\text{NiO}/\text{Ni}_3(\text{BO}_3)_2$ Nanocomposites to Advanced Photocatalytic Performance. *Arab. J. Chem.* **2022**, *15*, 103768. [[CrossRef](#)]
27. Aflaki, M.; Davar, F. Synthesis, luminescence and photocatalyst properties of zirconia nanosheets by modified Pechini method. *J. Mol. Liq.* **2016**, *221*, 1071–1079. [[CrossRef](#)]
28. Bayat, B.; Tahvildari, K.; Hemmati, A.; Bazyari, A.; Ghaemi, A. Production of ethylene glycol monobutyl ether through etherification of ethylene glycol using a nanostructured heterogeneous catalyst of amyberlyst-15. *Process Saf. Environ. Prot.* **2022**, *165*, 597–609. [[CrossRef](#)]
29. Mendelson, N.L.; Fitzgerald, A.; Kumar, A.; Pineda, J.A.; MacDougall, J.; Solomon, R.J.; Gibson, P.C.; Prikis, M.; Marroquin, C.E. Impact of Ethylene Glycol Toxicity on Donor Organ Viability: A Case Report. *Transplant. Proc.* **2017**, *49*, 2411–2414. [[CrossRef](#)]
30. Pirzadi, Z.; Meshkani, F. From glycerol production to its value-added uses: A critical review. *Fuel* **2022**, *329*, 125044. [[CrossRef](#)]
31. Durán, P.; Capel, F.; Gutierrez, D.; Tartaj, J.; Moure, C. Cerium (IV) Oxide Synthesis and Sinterable Powders Prepared by the Polymeric Organic Complex Solution Method. *J. Eur. Ceram. Soc.* **2002**, *22*, 1711–1721. [[CrossRef](#)]
32. Bodachivskiy, I.; Kuzhiumparambil, U.; Williams, D.B.G. Acid-Catalyzed Conversion of Carbohydrates into Value-Added Small Molecules in Aqueous Media and Ionic Liquids. *ChemSusChem* **2018**, *11*, 642–660. [[CrossRef](#)] [[PubMed](#)]
33. Dongsri, S.; Rattanaphanee, P.; Wongkoblaph, A. Production of Lactic Acid from Cellulose Using Solid Catalyst. *MATEC Web Conf.* **2019**, *268*, 07006. [[CrossRef](#)]
34. Qi, X.; Watanabe, M.; Aida, T.M.; Smith, R.L., Jr. Catalytic Dehydration of Fructose into 5-Hydroxymethylfurfural by Ion-Exchange Resin in Mixed-Aqueous System by Microwave Heating. *Green Chem.* **2008**, *10*, 799. [[CrossRef](#)]
35. Gomes, F.N.D.C.; Mendes, F.M.T.; Souza, M.M.V.M. Synthesis of 5-Hydroxymethylfurfural from Fructose Catalyzed by Phosphotungstic acid. *Catal. Today* **2017**, *279*, 296–304. [[CrossRef](#)]
36. Taghavi, S.; Ghedini, E.; Menegazzo, F.; Mäki-Arvela, P.; Peurla, M.; Zendejdel, M.; Cruciani, G.; Di Michele, A.; Murzin, D.Y.; Signoretto, M. CuZSM-5@HMS Composite as an Efficient Micro-Mesoporous Catalyst for Conversion of Sugars into Levulinic Acid. *Catal. Today* **2022**, *390*, 146–161. [[CrossRef](#)]
37. Yang, F.; Liu, Q.; Bai, X.; Du, Y. Conversion of Biomass into 5-Hydroxymethylfurfural Using Solid Acid Catalyst. *Bioresour. Technol.* **2011**, *102*, 3424–3429. [[CrossRef](#)]
38. Wei, W.; Yang, H.; Wu, S. Efficient Conversion of Carbohydrates into Levulinic Acid over Chromium Modified Niobium Phosphate Catalyst. *Fuel* **2019**, *256*, 115940. [[CrossRef](#)]
39. Tsilomelekis, G.; Orella, M.J.; Lin, Z.; Cheng, Z.; Zheng, W.; Nikolakis, V.; Vlachos, D.G. Molecular Structure, Morphology and Growth Mechanisms and Rates of 5-Hydroxymethyl Furfural (HMF) Derived Humins. *Green Chem.* **2016**, *18*, 1983–1993. [[CrossRef](#)]
40. Cantero, D.A.; Vaquerizo, L.; Martinez, C.; Bermejo, M.D.; Cocero, M.J. Selective Transformation of Fructose and High Fructose Content Biomass into Lactic Acid in Supercritical Water. *Catal. Today* **2015**, *255*, 80–86. [[CrossRef](#)]
41. Shen, D.K.; Gu, S. The Mechanism for Thermal Decomposition of Cellulose and Its Main Products. *Bioresour. Technol.* **2009**, *100*, 6496–6504. [[CrossRef](#)] [[PubMed](#)]
42. Fang, T.; Liu, M.; Li, Z.; Xiong, L.; Zhang, D.; Meng, K.; Qu, X.; Zhang, G.; Jin, X.; Yang, C. Hydrothermal Conversion of Fructose to Lactic Acid and Derivatives: Synergies of Metal and Acid/Base Catalysts. *Chin. J. Chem. Eng.* **2022**; *in press*. [[CrossRef](#)]

43. Kong, L.; Shen, Z.; Zhang, W.; Xia, M.; Gu, M.; Zhou, X.; Zhang, Y. Conversion of Sucrose into Lactic Acid over Functionalized Sn-Beta Zeolite Catalyst by 3-Aminopropyltrimethoxysilane. *ACS Omega* **2018**, *3*, 17430–17438. [[CrossRef](#)] [[PubMed](#)]
44. Lomate, S.; Katryniok, B.; Dumeignil, F.; Paul, S. High Yield Lactic Acid Selective Oxidation into Acetic Acid over a Mo-V-Nb Mixed Oxide Catalyst. *Sustain. Chem. Process.* **2015**, *3*, 5. [[CrossRef](#)]
45. Fang, Y.; Zeng, X.; Yan, P.; Jing, Z.; Jin, F. An Acidic Two-Step Hydrothermal Process To Enhance Acetic Acid Production from Carbohydrate Biomass. *Ind. Eng. Chem. Res.* **2012**, *51*, 4759–4763. [[CrossRef](#)]
46. Dos Santos, T.V.; Da Silva Avelino, D.O.; Pryston, D.B.A.; Meneghetti, M.R.; Meneghetti, S.M.P. Tin, molybdenum and tin-molybdenum oxides: Influence of Lewis and Bronsted acid sites on xylose conversion. *Catal. Today* **2021**, *394*, 125–132. [[CrossRef](#)]
47. Yousefi, T.; Khanchi, A.R.; Ahmadi, S.J.; Rofouei, M.K.; Yavari, R.; Davarkhah, R.; Myanji, B. Cerium(III) Molybdate Nanoparticles: Synthesis, Characterization and Radionuclides Adsorption Studies. *J. Hazard. Mater.* **2012**, *215*, 266–271. [[CrossRef](#)]
48. Nasser, H.; Rédey, Á.; Yuzhakova, T.; Kovács, J. Thermal Stability and Surface Structure of Mo/CeO₂ and Ce-Doped Mo/Al₂O₃ Catalysts. *J. Therm. Anal. Calorim.* **2009**, *95*, 69–74. [[CrossRef](#)]
49. Castellan, A.; Bart, J.C.J.; Bossi, A.; Perissinoto, P.; Giordano, N. On the Formation of Cerium Molybdates under different atmospheric and thermal conditions. *Z. Anorg. Allg. Chem.* **1976**, *422*, 155–172. [[CrossRef](#)]
50. Khalil, K.M.S.; Elkabee, L.A.; Murphy, B. Preparation and Characterization of Thermally Stable Porous Ceria Aggregates Formed via a Sol-Gel Process of Ultrasonically Dispersed Cerium(IV) Isopropoxide. *Micropor. Mesopor. Mater.* **2005**, *78*, 83–89. [[CrossRef](#)]
51. Suresh, R.; Ponnuswamy, V.; Mariappan, R. Effect of Annealing Temperature on the Microstructural, Optical and Electrical Properties of CeO₂ Nanoparticles by Chemical Precipitation Method. *Appl. Surf. Sci.* **2013**, *273*, 457–464. [[CrossRef](#)]

Disclaimer/Publisher’s Note: The statements, opinions and data contained in all publications are solely those of the individual author(s) and contributor(s) and not of MDPI and/or the editor(s). MDPI and/or the editor(s) disclaim responsibility for any injury to people or property resulting from any ideas, methods, instructions or products referred to in the content.